ELSEVIER

Journal of Molecular Catalysis A: Chemical 137 (1999) 223–237

JOURNAL OF MOLECULAR CATALYSIS A: CHEMICAL

Zeolite-encapsulated vanadium picolinate peroxo complexes active for catalytic hydrocarbon oxidations

Alexander Kozlov [a], Anguelina Kozlova [a], Kiyotaka Asakura [b], Yasuhiro Iwasawa [a,*]

[a] *Department of Chemistry, Graduate School of Science, The University of Tokyo, Hongo, Bunkyo-ku, Tokyo 113, Japan*
[b] *Research Center for Spectrochemistry, Faculty of Science, The University of Tokyo, Hongo, Bunkyo-ku, Tokyo 113, Japan*

Received 17 January 1998; accepted 3 April 1998

Abstract

Zeolite-encapsulated vanadium (IV) picolinate complexes were prepared by treatment of dehydrated VO(2 +)–NaY zeolite with molten picolinic acids. Treatment of the NaY-encapsulated $VO(pic)_2$ complex with urea hydrogen peroxide adduct in acetonitrile allowed to generate peroxovanadium species. The structure of vanadium peroxo species was studied by UV–vis, Raman and XAFS spectroscopies which suggested the formation of monoperoxo monopicolinate complex which could be active intermediate for various oxidation reactions with the catalysts. To elucidate effect of the encapsulation on catalytic performance, the catalytic properties of the encapsulated complexes were compared with that of corresponding homogeneous catalyst $H[VO(O_2)(pic)_2] \cdot H_2O$. The novel 'ship-in-a-bottle' catalysts retain solution-like activities in aliphatic and aromatic hydrocarbon oxidations as well as in alcohol oxidation. In addition, the encapsulated vanadium picolinate catalysts showed a number of distinct features such as preferable oxidation of smaller substrates in competitive oxidations, increased selectivity of the oxidation of terminal CH_3- group in isomeric octanes and preferable (sometimes exclusive) formation of alkyl hydroperoxides in alkane oxidations. The distinct features were explained in terms of intrazeolitic location of the active complexes that imposed transport discrimination and substrate orientation. On the basis of the experimental data, a possible mechanism was discussed. Stability of the vanadium complexes during the liquid phase oxidations and leaching from the NaY zeolite matrix were also examined.

Keywords: Encapsulated vanadium complexes; Zeolite Y; Oxidation reactions; Alkanes; Peroxo intermediates; Raman spectroscopy; XAFS; UV–vis spectroscopy

1. Introduction

Selective catalytic oxidations of various organic substrates by transition metal modified zeolites are of scientific and industrial interests [1–4]. One of new perspective directions involves catalysis by so-called 'ship-in-a-bottle' complexes. This strategy suggests heterogenization of transition metal complexes with potential catalytic activity in zeolites or other molecular sieves, where complexes are fixed due to spatial restrictions, Coulombic interactions or covalent bondings [5–8]. This approach has been successfully applied to synthesis of a variety of transition metal complexes in synthetic faujasite (FAU and EMT topologies), NaA, VPI-5, ZSM-

* Corresponding author. Fax: +81-3-5800-6892; e-mail: iwasawa@chem.s.u-tokyo.ac.jp

1381-1169/99/$ - see front matter
PII: S1381-1169(98)00128-9

5, ZSM-51, $AlPO_4$-5, $AlPO_4$-11, nonasil, FSM-16, MCM-41 molecular sieves. The ability of the new materials to activate molecular oxygen and reduced forms of oxygen such as hydrogen peroxide and *tert*-butyl hydroperoxide and performance of the catalysts in liquid-phase oxidations have extensively been studied. However, most of publications have been concerned with catalysts for electrophilic oxygen transfer, especially, for alkene epoxidation [5,8–10]. On the other hand, there are only a few reports about radical-based hydroxylation of hydrocarbons using zeolite-encapsulated complexes.

Vanadium (V) in an aqueous solution of hydrogen peroxide can react with pyridine- and pyrazine-2-carboxylic acids, resulting in relatively stable peroxovanadium carboxylato complexes. These complexes show enhanced reactivity toward homolytic oxygen transfer to hydroxylate aromatic and aliphatic hydrocarbons under mild conditions [11–13]. Shul'pin and Süss-Fink [14] and Shul'pin et al. [15] designed a catalytic process in an acetonitrile solution of H_2O_2 with *t*-Bu_4NVO_3 and pyrazine- or pyridine-2-carboxylic acids as in situ catalyst precursors.

Recently, we reported synthesis of vanadium (IV) complexes with picolinic acids encapsulated inside NaY zeolite supercages by a flexible ligand method which involved the treatment of a VO(2 +)–NaY zeolite with molten picolinic acids followed by Soxhlet extraction to remove excess of the ligands and complexes located on external surfaces of the zeolite [16,17]. Formation of bispicolinate vanadium complexes with distorted octahedral coordination was concluded from characterization of the encapsulated species by EXAFS, XANES, FT-IR, ESR and UV–vis spectroscopies. The vanadium (IV) complexes were suggested to be located in the zeolite supercages by XRD as well as comparative XPS/XRF studies. Despite high thermal stability of the encapsulated complexes, the attempts to use the materials as catalysts for gas phase oxidations were unsuccessful. On the other hand, the encapsulated V(IV) picolinates could be precursors for encapsulated peroxovanadium pyridine-2-carboxylato complexes that are potentially effective catalysts for a variety of liquid phase oxidations. The present research is concerned with generation of peroxovanadium pyridine-2-carboxylato complexes in NaY zeolite supercages. The catalytic performance of encapsulated vanadium picolinate complexes in oxidations of hydrocarbons and alcohols with urea hydrogen peroxide adduct under anhydrous conditions was tested. Effects imposed by intrazeolitic location of the vanadium complex on the reaction selectivities were elucidated by a series of experiments with heterogeneous encapsulated vanadium picolinate catalysts and homogeneous $H[VO(O_2)(pic)_2] \cdot H_2O$ catalyst. On the basis of the experimental data, a mechanism of alkane oxidation was discussed. Particular attention was paid to the stability of the catalysts.

2. Experimental

2.1. Materials

The starting vanadium compound $VOSO_4 \cdot nH_2O$ ($n = 3$–4) (purity 99.9%) was purchased from Wako Pure Chemical Industries (Wako). Picolinic acid (picH) (99%), quinaldic acid (QpicH) (99%), 5-*n*-butyl-2-picolinic acid (BupicH) (95%) were received from Soekawa Chemicals. Pyridine (99.5%, Wako) and acetonitrile (99.5%, Wako) were used as solvents for Soxhlet extraction. Reaction studies were carried out with dehydrated acetonitrile (99.0%, Wako). Urea hydrogen peroxide adduct, UHP (98%, Aldrich), hydrogen peroxide (31% in water, Wako) and *t*-BuOOH (5–6 mol l^{-1} solution in decane, Aldrich) were used as oxidants. Authentic samples for gas chromatographic analysis (all EP grade) were received from Soekawa Chemicals. NaY zeolite with a Si/Al ratio of 5.6 was supplied by Tosoh (HSZ-320NAA, Lot. 3001) and pretreated before use according to literature [18].

2.2. Samples preparation

Vanadium (IV) complexes and vanadium (V) peroxo complexes with picolinic acids were synthesized as described in the literature [13,19].

Encapsulated samples $VO(PL)_2$–NaY (namely, $VO(pic)_2$–NaY (HL), $VO(Bupic)_2$–NaY (HL), $VO(Qpic)_2$–NaY (HL), $VO(pic)_2$–NaY (LL), $VO(Qpic)_2$–NaY (LL)) were prepared in a similar manner to that reported previously [17]. HL and LL abbreviations are used hereinafter for high loading (~ 0.8 vanadium per supercage) and low loading (~ 0.2 vanadium per supercage) samples, respectively. In a typical experiment, 4 g of a dehydrated form of VO(2 +)–NaY zeolite precursor was treated with 10 g of molten picolinic (or substituted picolinic) acid at 433 K for 6–10 h under argon (99.9999% purity) atmosphere. Then the sample was Soxhlet extracted with pyridine for 60 h followed by additional Soxhlet extraction with acetonitrile for 48 h and finally dried in vacuum at 298 K for 4 h.

2.3. Spectroscopic characterization

ESR spectra for powdered samples were measured at room temperature on a JES-RE2X spectrometer. The microwave power was 1.00 mW with a resonance frequency of 9.1 GHz (X-band). The g values were determined relatively to DPPH ($g = 2.0036$). Signal intensities were calculated by double integration of the ESR signals.

In situ UV–visible diffuse reflectance spectra in the region 250–900 nm were recorded on a Hitachi U-3500 spectrometer using a quartz cell for self-supporting disks at room temperature in air. Disks of NaY zeolite and $VO(pic)_2$–NaY (HL) were used as references.

V K-edge XAFS (X-ray absorption fine structure) spectra for the vanadium samples and a mixture of a reference compound and boron nitride which were pressed into self-supporting disks were measured at the BL-7C station of the Photon Factory in the National Laboratory for High Energy Physics (KEK-PF) with a positron energy of 2.5 GeV and a storage ring current 250–350 mA (Proposal No. 95G199). A synchrotron radiation was monochromatized by a Si(111) sagittal focusing double crystal. Higher harmonics were removed by using a total-reflection double mirror and detuning the parallelism for the intensity to be 60% of the maximum. V K-edge spectra were recorded in a transmission mode using ionization chambers filled with flowing N_2 for I_0 and I as X-ray detectors. To perform in situ EXAFS measurements, a self-supporting disk of $VO(pic)_2$–NaY (HL) was placed into polyethylene packet filled with acetonitrile solution of UHP. The EXAFS data were analyzed by the EXAFS analysis program 'Rigaku EXAFS (REX)' [20]. Fourier transforms range was 3.5–13.5 $Å^{-1}$.

Quantification of vanadium in samples was performed using energy dispersive X-ray fluorescence (XRF) on a Seiko SII SEA2010, equipped with a rhodium source for X-rays, a series of secondary targets and Si (Li) drift detector. The calibration curve was obtained by using NaY zeolites impregnated with given amounts of $VO(acac)_2$.

Raman spectra were recorded with a Renishaw Raman Microscope; a He–Ne laser providing light wavelength 632 nm was used as the excitation source. The spectra of powder samples were taken at ambient conditions. The laser power at the sample was 30 mW.

2.4. Catalytic performance

Liquid phase oxidations were performed in thermostated cylindrical vessels at 298 K in air under vigorous stirring. Addition of a catalyst was considered to be the starting point of the reaction. Reaction solutions were analyzed before and after treatment with excess of triphenylphosphine [15] by temperature programmed GC chromatography analyses by using a 6-m column of 15% Unisole 30 T on Uniport HP (for oxidation of alkanes, alcohols and cyclohexene), a 2-m column of KG-02 on Uniport

HP (for oxidation of aromatic hydrocarbons), and a 3-m column of 15% Silicone DC200 on Uniport HP (for competitive oxidations and oxidation of cyclohexene). In a typical experiment, 6 mmol of UHP ($H_2O_2 \cdot$ urea adduct) (0.57 g) was added to 10 ml of dehydrated acetonitrile containing 3 mmol of a substrate. After saturation of the solution with UHP, 3×10^{-2} mmol of the vanadium complex (120 mg of $VO(PL)_2$–NaY (HL), 480 mg of $VO(PL)_2$–NaY (LL) or 11 mg of $H[VO(O_2)(pic)_2] \cdot H_2O$) was added to the reaction mixture.

2.5. Heterogeneous character of the catalysis

Heterogeneous character of the catalysis was investigated in the case of cyclohexane. Three runs were conducted simultaneously. In 'Continuous' and 'Filtration' experiments, both cyclohexane and UHP were added to acetonitrile before the starting point of the reaction. When cyclohexane conversion reached approximately 3–6% (reaction time 5 h), the catalyst and the oxidant were removed from one of the reaction mixtures by filtration over a glass microfibre filter and then a fresh portion of the oxidant was introduced. In a 'Leaching' experiment, the only oxidant (UHP) was added to acetonitrile before introduction of the catalyst. Thus, detachment of the complex from the zeolite was carried out in the absence of the substrate. After 5-h reaction, the catalyst and UHP were removed from the reaction mixture by filtration over a glass microfibre filter, followed by addition of cyclohexane and a new portion of UHP. 'Spent' and 'Spent 2' experiments were performed in a manner similar to 'Continuous' experiment with catalysts, extensively washed with acetonitrile after 'Continuous' and 'Spent' experiments, respectively. Total reaction time was 10 h for all the experiments. Typically, the reactions were performed with 20 mmol of UHP (1.88 g), 6 mmol of cyclohexane and 2×10^{-2} mmol of a catalyst in 20 ml of dehydrated acetonitrile at 313 K.

2.6. Competitive oxidations

Competitive oxidations were carried out with the following pairs of substrates; cyclooctane: cyclodecane, toluene: 1,3-di-*t*-butylbenzene, and *n*-octane: 2,5-dimethylhexane. In a typical experiment, 10 mmol of UHP (0.94 g) was added to 20 ml acetonitrile solution which contained one pair of the substrates (1 mmol each). After saturation of the solution with UHP, 80 mg of $VO(pic)_2$–NaY (HL) (2×10^{-2} mmol of the $VO(pic)_2$ complex), or 7 mg of $H[VO(O_2)(pic)_2] \cdot H_2O$ (2×10^{-2} mmol) was introduced into the former mixture. The oxidation reactions were performed at 313 K for 10 h.

2.7. Regioselective oxidations

Regioselective oxidations were also studied by using *n*-hexane, *n*-octane and 2,5-dimethylhexane oxidation reactions as substrates. Reaction conditions were the same as those described in Sections 2–4.

3. Results

3.1. Formation of peroxovanadium complexes in NaY supercages

ESR spectra of the $VO(pic)_2$–NaY (HL) zeolite before (curve (a)) and after (curve (b), (c)) treatment with an acetonitrile solution of UHP are shown in Fig. 1. Gradual decrease in ESR signal intensity of $VO(pic)_2$–NaY (HL) was observed upon the treatment of the sample without changes in g and A parameters ($g_{\|} = 1.945$, $g_{\perp} = 1.996$, $A_{\|} = 175.3$ G, and $A_{\perp} = 67.1$ G). After 2 h of the treatment, about 50% of the vanadyl complex was oxidized to V(+5), but even after 24 h of the treatment, 10% of vanadium retained the oxidation state of +4. Reverse growth in the ESR signal intensity occurred when UHP was exhausted, probably due to decomposition of peroxo complexes produc-

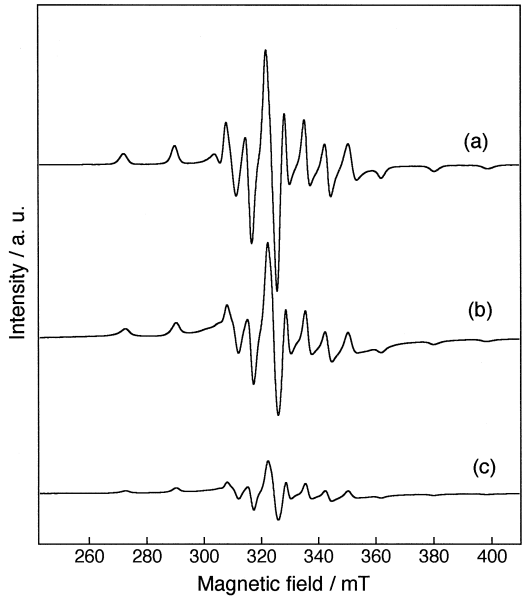

Fig. 1. ESR spectra of the encapsulated $VO(pic)_2$–NaY (HL) sample: (a) as synthesized and after treatment with an acetonitrile solution of UHP for (b) 2 h, (c) 24 h.

ing the initial bispicolinate complex and oxygen. Treatment of the $VO(pic)_2$–NaY (IM) sample with UHP resulted in complete oxidation of the V(+4) picolinate and a new ESR signal of low intensity with fine structure was detected ($g = 2.011$, $A = 4.3$ G). The fine structure consisted of eight lines. Low value of the splitting constant argues for formation of radical species interacted with V(+5) center and the signal could be attributed to V(+5)–·OOH species [21].

Diffuse reflectance spectra in UV–visible region for the $VO(pic)_2$–NaY (HL) samples treated with UHP together with untreated one are shown in Fig. 2. The spectra were referred to NaY zeolite (upper figure) and $VO(pic)_2$–NaY (HL) sample (lower figure). Growth of the peak intensity centered at 475 nm was observed. It is known that vanadium can form monoperoxo and diperoxo complexes, which show characteristic absorption bands at 450–480 nm and 320–340 nm, respectively [22]. The UV data allows to suggest the oxidation of the encapsulated $VO(pic)_2$ complex to form monoperoxo species upon treatment with UHP.

Raman spectra of NaY zeolite (Fig. 3a) showed only an intense band at 500 cm^{-1} that can be assigned to a bending vibration of Si–O–Si bond. Two other low-intensity bands near 800 cm^{-1} and 1100 cm^{-1} can be described as symmetric and asymmetric stretching modes ν_s (SiO) and ν_{as} (SiO), respectively [23,24]. The typical bands of V=O, $V–O_p$ (peroxo) and O–O vibrations in vanadium(+5) peroxo complexes are observed at 920–1000, 660–490 and 800–940 cm^{-1}, respectively [25–28]. Thus, Raman spectroscopy can be considered as a feasible technique for characterization of the encapsulated vanadium peroxo complexes. Raman spectra for a number of reference compounds were measured and are summarized in Table 1, where selected literature data for vanadium peroxo complexes are listed. Vanadium(+4) picolinates exhibited V=O stretching at 967 cm^{-1}

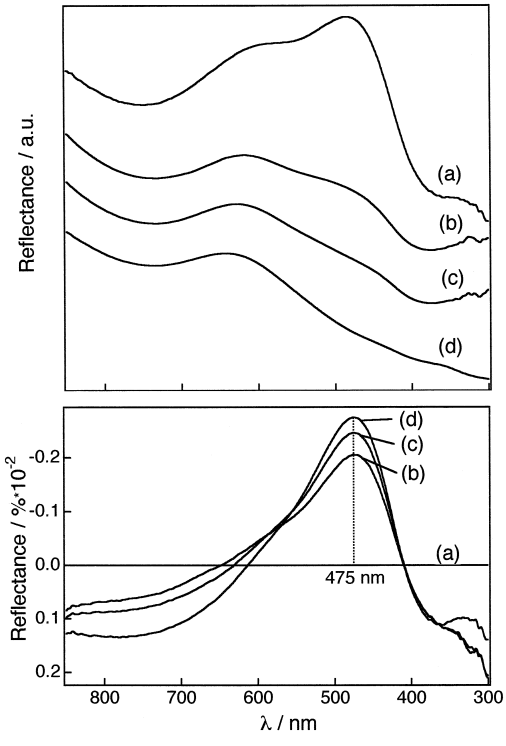

Fig. 2. Diffuse reflectance spectra of the encapsulated $VO(pic)_2$–NaY (HL) sample: (a) as synthesized, and treated with an acetonitrile solution of UHP for (b) 30 min, (c) 2 h, and (d) 24 h. The spectra were measured in situ and referred to NaY zeolite (upper) or $VO(pic)_2$–NaY (HL) sample (lower).

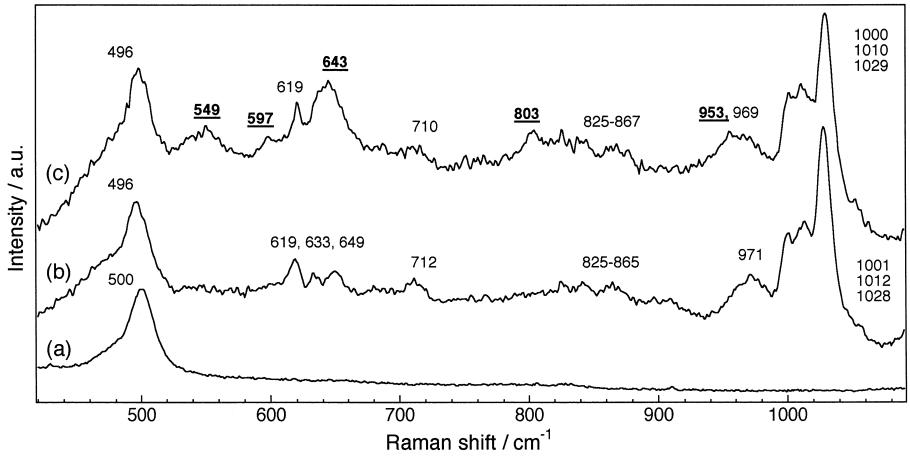

Fig. 3. Raman spectra of (a) NaY zeolite and the encapsulated $VO(pic)_2$–NaY (HL) sample: (b) as synthesized and (c) after treatment with an acetonitrile solution of UHP.

($VO(pic)_2 \cdot H_2O$) and 958 cm^{-1} ($VO(pic)_2(py)$). Bands near 1020 cm^{-1} in both V(+4) and V(+5) complexes are assigned to the picolinic ligand. The band position is shifted in comparison with uncomplexed picH that shows very strong band at 1032 cm^{-1} and two medium-strong bands at 992 and 1005 cm^{-1}. V–N stretching was observed in the 450–480 cm^{-1} region as shown in Table 1. Vanadium(+5) peroxo complexes containing aminocarboxylate ligands show the O–O distance of 1.39–1.435 Å and ν(O–O) of 935–940 cm^{-1} (Table 1) [25,28]. The band can be partially overlapped with V=O stretching (950–970 cm^{-1}). On the other hand, a number of stable oxodiperoxovanadates were isolated from H_2O_2 solution containing NH_3, F^-, $C_2O_4^{2-}$ and CO_3^{2-} ligands. These compounds exhibit the O–O distance of 1.455–1.487 Å and show strong ν(O–O) stretching peak in the range 876–896 cm^{-1} [27,28]. The V=O stretching lies between 950 and 970 cm^{-1}. Thus, Raman spectroscopy enables to distinguish the two types of vanadium complexes. In addition, we expected to identify monopicolinate and bispicolinate peroxo species by comparison of the band intensities. In the course of the Raman investigation, we observed that positions of intensive bands were similar for monopicolinate and bispicolinate peroxo complexes (Table 1). The only difference was the position of $V–O_p$ ($\sim$ 540 cm^{-1}) that could be assigned to symmetric stretching of V–O bond. However, relative intensities of the bands differ significantly.

Raman spectra of the as-synthesized $VO(pic)_2$–NaY (HL) and $VO(pic)_2$–NaY (HL) sample treated with an acetonitrile solution of UHP are shown on Fig. 3b,c, respectively. The most prominent peak characteristic of NaY is located at 496 cm^{-1}. The small shift in comparison with the starting NaY zeolite may be explained by replacement of a part of the Na cations by encapsulated vanadium picolinate complex [23]. Stretching vibration of V–N bonds is obscured by the bending vibration of Si–O–Si bond and appears as a shoulder at about 450–470 cm^{-1}. The new intensive bands in the spectrum of the $VO(pic)_2$–NaY (HL) sample were observed at 971, 1001, 1012, and 1028 cm^{-1}. The position of the first band (971 cm^{-1}) is similar to one for $VO(pic)_2 \cdot H_2O$ (967 cm^{-1}, Table 1) and corresponds to V=O stretching. However, there is significant difference (27 cm^{-1}) in the band position as compared to VO(2+)–NaY precursor (998 cm^{-1}). The other three bands in the spectrum of the $VO(pic)_2$–NaY (HL) sample are ascribed to vibrations of the picolinic ligands. The main

Table 1
Raman bands (cm^{-1}) for selected vanadium complexes

Sample	ν(V=O)	ν(O–O)	ν(V–O_p)	ν(V–N)	Other strong bands	Reference
$VO(pic)_2 \cdot H_2O$	967s	–	–	452w	650m, 1026vs	this work
$VO(pic)_2(py)$	958s	–	–	430w, 459w	647m, 1011vs, 1025vs	this work
$VO(O_2)(pic) \cdot 2H_2O$	969s	934m	549vs, 586w, 645m	451w, 479s	678s, 977m, 1029m	this work
$H[VO(O_2)(pic)_2] \cdot H_2O$	966s	939sh	537m, 589m, 645m	452, 458sh	706m, 1025vs	this work
$[VO(pic)]_2O_2 \cdot H_2O$	984s	–	–	450sh, 462sh	480s, 611s, 991s, 1020s, 1027s	this work
$K_3[VO(O_2)_2C_2O_4] \cdot H_2O$	924vs	876s, 859w	631m, 584s, 485vs, 472sh	–	520s	[27]
$NH_4[VO(O_2)_2(NH_3)]$	1000m, 957vs	884s	623m, 533vs, 503m	446m	–	[27]
$K_2[VO(HEDTA)(O_2)] \cdot 4H_2O$	953vs	940sh	562s	451m	–	[25]
$K_3[V(O_2)_4]$	–	859(10)	623(5), 576(6)	–	–	[26]
$[VO_4]^{3-}$ in 2.5 mol/l H_2O_2 pH < 6.0	975–987	873–893	624–630(1–2), 535–545(10), 476–500(1–2)	–	–	[26]

band at 1028 cm^{-1} is close to the picolinic ligand band at 1026 cm^{-1} in $VO(pic)_2 \cdot H_2O$ (Table 1). The other two bands arose from the presence of small amounts of $VO(pic)_2(py)$ complex and picH adsorbed on the zeolite. Several low intensive bands occurred in 615–715 cm^{-1} and 825–865 cm^{-1} regions. Raman spectrum of the $VO(pic)_2$–NaY (HL) sample treated with an acetonitrile solution of UHP (Fig. 3c) shows appearance of new bands in the $V–O_p$ region at 549, 597, and 643 cm^{-1}. In addition, shift and broadening of the V=O stretching around 960 cm^{-1} due to overlapping with O–O vibration were observed. A new band at 803 cm^{-1} was tentatively assigned to a product of decomposition of vanadium peroxo complexes or to a vanadium μ-peroxo complex.

XANES spectra for $VO(pic)_2$–NaY (HL) sample before and after treatment with an acetonitrile solution of UHP are presented in Fig. 4, together with spectra of reference peroxo compounds. The pre-edge peak for $VO(pic)_2$–NaY (HL) treated with UHP (Fig. 4b) was at 5468.4 eV which was higher by ~ 0.5 eV than that for the untreated $VO(pic)_2$–NaY (HL) sample (Fig. 4a). Shift of the pre-edge peak (the value is higher by ~ 4.5 eV than that for vanadium foil) reflects the oxidation of $V(+4)$ to $V(+5)$ [29]

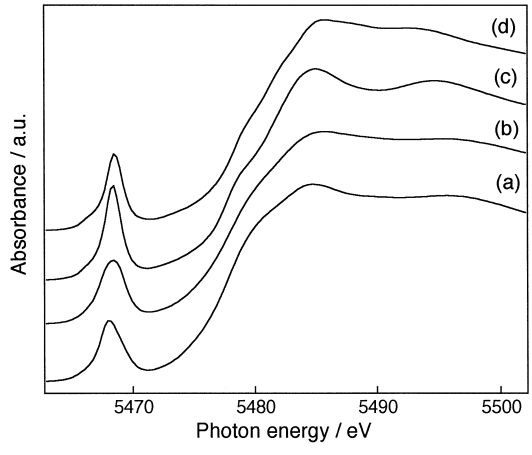

Fig. 4. Vanadium K-edge XANES spectra of (a) $VO(pic)_2$–NaY (HL) as synthesized, (b) $VO(pic)_2$–NaY (HL) treated in situ with an acetonitrile solution of UHP, (c) $H[VO(O_2)(pic)_2 \cdot H_2O/BN$, and (d) $VO(O_2)(pic) \cdot 2H_2O/BN$.

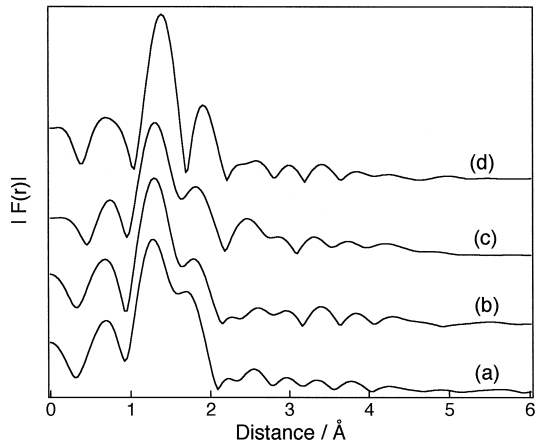

Fig. 5. Fourier transforms of the k^3-weighted EXAFS data for (a) $VO(pic)_2$–NaY (HL) as synthesized, (b) $VO(pic)_2$–NaY (HL) treated in situ with an acetonitrile solution of UHP, (c) $H[VO(O_2)(pic)_2 \cdot H_2O/BN$, and (d) $VO(O_2)(pic) \cdot 2H_2O/BN$.

by the treatment of the sample UHP. The reference compounds showed the $1s \rightarrow 4p$ transition peak at 5485.0 eV for $H[VO(O_2)(pic)_2] \cdot H_2O$ (Fig. 4c) and 5485.7 eV for $VO(O_2)(pic) \cdot 2H_2O$ (Fig. 4d).

EXAFS spectra at V K-edge were taken for the as synthesized $VO(pic)_2$–NaY (HL), the $VO(pic)_2$–NaY (HL), treated in situ with an acetonitrile solution of UHP, $H[VO(O_2)(pic)_2] \cdot H_2O/BN$ and $VO(O_2)(pic) \cdot 2H_2O/BN$. Fourier transforms of the k^3-weighted EXAFS data are shown in Fig. 5. No V–V bonding was observed. The Fourier transforms for $H[VO(O_2)(pic)_2] \cdot H_2O/BN$ and $VO(O_2)(pic) \cdot 2H_2O/BN$(Fig. 5a,b) showed two major peaks which are straightforwardly assigned to V=O (1.60 Å) and V–O + V–N (1.8–2.15 Å), respectively.

3.2. Catalytic performance of the catalysts

It was found that cyclohexane oxidation with UHP was catalyzed by both heterogeneous $VO(pic)_2$–NaY (HL) and homogeneous $H[VO(O_2)(pic)_2] \cdot H_2O$ catalysts. Cyclohexyl hydroperoxide was the main reaction product with both catalysts, but the cyclohexyl hydroperoxide-to-cyclohexanone molar ratio was larger over the heterogeneous catalyst, where

Table 2
Catalytic oxidation of *n*-octane

Catalyst	Conversion (%)	Ketones/alcohols	Pos. 4/Pos. 1	Pos. 4/Pos. 2	Reference
$VO(pic)_2$–NaY (HL)[a]	19.9	0.05	4.1	0.92	this work
$VO(pic)_2$–NaY (LL)[a]	19.5	0.04	4.2	0.96	this work
$VO(Qpic)_2$–NaY (LL)[a]	5.9	0.04	4.0	0.97	this work
$H[VO(O_2)(pic)_2]*H_2O$[a]	22.6	0.73	5.2	0.96	this work
VS-1[b]	8.7	1.86	2.1	0.82	[30]
VS-2[c]	12.8	2.47	2.3	0.64	[31]
V-NCL-1[c]	25.6	2.98	3.6	0.67	[32]
CrS-1[b]	7.7	0.99	1.7	0.38	[30]
TS-1[d]	–[e]	0.58	–[f]	0.22	[33]

[a] Reaction conditions: catalyst 3×10^{-2} mmol, $H_2O_2\cdot$ urea adduct 6 mmol, *n*-octane 3 mmol, acetonitrile dehydrated 10 ml, 298 K, 24 h (reaction time for $H[VO(O_2)(pic)_2]\cdot H_2O$ catalyst 2 h).
[b] Reaction conditions: catalyst 0.5 g, *t*-BuOOH 3.95 g, *n*-octane 5 g, acetonitrile 25 ml, 373 K, 10 h.
[c] Reaction conditions: catalyst 0.1 g, *n*-octane 5 g, *n*-octane/H_2O_2 (26%) = 3 (mole ratio), acetonitrile 10 g, 373 K, 8 h.
[d] Reaction conditions: catalyst 0.856 g, 0.307 mol/l H_2O_2 50 ml in 95% methanol, *n*-octane 5.8 ml, 328 K.
[e] $t_{1/2}$ = 57 min (50% conversion of H_2O_2), yield (on H_2O_2) 63%.
[f] No products of oxidation of terminal CH_3– group was detected.

the ratio reached the value of 20. Alicyclic alkanes were also oxidized in the presence of both types of the catalysts. Regioselectivity in *n*-hexane oxidation was similar between homogeneous and heterogeneous catalysts. The data for the oxidation of *n*-octane and 2,5-dimethylhexane are summarized in Tables 2 and 3. Noticeable difference of regioselectivity between $H[VO(O_2)(pic)_2]\cdot H_2O$ and $VO(pic)_2$–NaY (HL) catalysts in the oxidation of isomeric C_8 alkanes (*n*-octane and 2,5-dimethylhexane) was observed. In *n*-octane oxidation on the $VO(pic)_2$–NaY (HL) catalyst regioselective oxidation at C_1 position increased $\sim$20% as compared with that on $H[VO(O_2)(pic)_2]\cdot H_2O$. More significant effects by use of the heterogeneous catalyst occurred in 2,5-dimethylhexane oxidation. The encapsulated $VO(pic)_2$ complex exhibited two times larger product ratio of position 1/position 3 than the homogeneous system. Relative amounts of ketones were higher for the homogeneous catalyst than for heterogeneous catalyst in the oxidations of both *n*-octane and 2,5-dimethylhexane.

Benzene was hydroxylated to phenol. Toluene was converted to a mixture of benzyl alcohol, benzaldehyde and isomeric cresols. Relative ratios of nucleus and chain oxidations were similar for both homogeneous and heterogeneous catalysts (43% of chain oxidation and 57% of aromatic ring oxidation). Both catalytic systems effectively converted cyclohexanol and 2-propanol into cyclohexanone and acetone, respectively. Cyclohexene underwent the oxidations of

Table 3
Catalytic oxidation of 2,5-dimethylhexane[a]

Catalyst	Conversion (%)	Ketones/alcohols	Pos. 3/Pos. 1	Pos. 3/Pos. 2
$VO(pic)_2$–NaY (HL)	21.8	0.00	1.61	0.41
$VO(pic)_2$–NaY (LL)	20.1	0.00	1.35	0.21
$VO(Bupic)_2$–NaY (HL)	15.7	0.00	1.76	0.37
$VO(Qpic)_2$–NaY (HL)	4.5	0.00	2.22	0.41
$VO(Qpic)_2$–NaY (LL)	5.9	0.00	1.34	0.30
$H[VO(O_2)(pic)_2]\cdot H_2O$	26.6	0.06	2.56	0.36

[a] See footnotes to Table 2.

Table 4
Catalytic oxidation of cyclohexane on encapsulated vanadium (IV) picolinates[a]

Catalyst	Experiment	Products[b] (mmol)				Activity[c] (mol mol V^{-1} h^{-1})	Hetero/homo
		2 h	5 h	8 h	10 h		
$VO(pic)_2$–NaY (HL)	Continuous	0.313	0.922	1.568	1.940		
	Filtration	0.318	0.912	1.174	1.360		
	Leaching	–	0.000	0.182	0.274	9.7	1.2
	Spent	–	–	–	1.600		
	Spent 2	–	–	–	1.060		
$VO(pic)_2$–NaY (LL)	Continuous	0.320	0.950	1.502	1.922		
	Filtration	0.336	0.946	1.130	1.284	9.6	1.9
	Leaching	–	0.000	0.286	0.490		
$VO(Qpic)_2$–NaY (LL)	Continuous	0.136	0.332	0.488	0.614		
	Filtration	0.134	0.346	0.398	0.422	3.1	2.3
	Leaching	–	0.000	0.038	0.068		

[a]Reaction conditions: catalyst 2×10^{-2} mmol of complex, $H_2O_2 \cdot$ urea adduct 20 mmol, cyclohexane 6 mmol, acetonitrile dehydrated 20 ml, 313 K.
[b]Cyclohehyl hydroperoxide > 90%.
[c]Activity of $H[VO(O_2)(pic)_2] \cdot H_2O$ catalyst was ~80 mol mol V^{-1} h^{-1}.

both allylic C–H bond and double C=C bond. Product distribution was 62% (C–H) and 38% (C=C) for the oxidation with $H[VO(O_2)(pic)_2] \cdot H_2O$ while a mixture of 70% (C–H) and 30% (C=C) was produced on heterogeneous $VO(pic)_2$–NaY (HL) catalyst.

3.3. Competitive oxidations

Competitive oxidations were performed for the following selected pairs of hydrocarbons: cyclooctane/cyclodecane, toluene/1,3-di-*t*-butylbenzene, and *n*-octane/2,5-dimethylhexane. The rates of oxidation of the smaller substrates increased on 14, 15 and 6%, respectively, relatively to those of the larger ones by application of the heterogeneous catalyst $VO(pic)_2$–NaY (HL) instead of the homogeneous catalyst $H[VO(O_2)(pic)_2] \cdot H_2O$.

3.4. Stability of encapsulated vanadium picolinate catalysts

Stability of the vanadium picolinate catalysts during liquid phase oxidations was studied in cyclohexane oxidation. The amounts of products as a function of reaction time in 'Continuous', 'Filtration', 'Leaching' and 'Spent' experiments on three different encapsulated catalysts are summarized in Table 4. The initial reaction rates were similar for 'Continuous' and 'Filtration' runs. The reaction rate for product accumulation decreased for the second run ('Filtration' in Table 4) after removal of the catalyst from the reaction mixture. Heterogeneous part of the reaction was estimated by subtracting the average reaction rate of 'Filtration' and 'Leaching' experiments from that of 'Continuous' experiment. The heterogeneous part decreased as follows for the catalysts: $VO(Qpic)_2$–NaY (LL) (70%) > $VO(pic)_2$–NaY (LL) (65%) > $VO(pic)_2$–NaY (HL) (55%). It should be noted that the part of homogeneous phase reaction increased up to 70–80% when the reaction was carried out at 323–333 K. Spent catalyst showed 15–20% loss of the activity after each recycle.

4. Discussion

4.1. Choice of an oxidant

Catalytic oxidations with metal complexes proceed through oxometal and peroxometal species [34] which dictates choice of an oxidant. The character of oxo and peroxo metal species

is affected by nature of both metal and ligand. Key reaction intermediates in catalytic liquid phase oxidations with vanadium pyridine- and pyrazine-2-carboxylate complexes include peroxo complexes that can effectively hydroxylate hydrocarbons [11,12]. The peroxo complexes could be generated in zeolite pores by treatment of the encapsulated V(+4) complexes using hydrogen peroxide and *t*-BuOOH. Treatment of $VO(pic)_2$–NaY (HL) with 5% *t*-BuOOH solution in acetonitrile did not result in oxidation of the zeolite encapsulated V(+4) complex according to ESR data and the $VO(pic)_2$–NaY-*t*-BuOOH system was found to be catalytically inactive for the oxidation of cyclohexane and cyclohexene at 323 K. On the contrary, use of 5% H_2O_2 solution instead of *t*-BuOOH caused fast oxidation of V(+4) species that was evidenced by the reduction in the ESR signal intensity (Fig. 1) and the change of sample color from greenish-blue to orange. Unfortunately, it was found that the treatment conditions imposed detachment of the complexes ($\sim$30%) into solution. It may be caused by partial hydrolysis of peroxo bispicolinate complexes in water-containing solutions. To suppress the leaching, the catalytic experiments were carried out under anhydrous conditions using hydrogen peroxide urea adduct $H_2O_2 \cdot (NH_2)_2CO$ (denoted as UHP) as a source of H_2O_2 [14,35,36].

4.2. Formation of peroxovanadium complexes

The ESR study revealed the gradual oxidation of encapsulated V(+4) picolinates to V(+5) complexes. The presence of considerable amounts of V(+4) does not allow to monitor radical species on V(+5) center. Instead, information about structure of V(+5) complexes formed upon the treatment of the V(+4) samples with UHP was obtained from UV, Raman and XANES measurements. A strong evidence for formation of vanadium monoperoxo complexes was obtained from in situ UV–vis spectra, where growth of the peak intensity centered at 475 nm was observed upon the treatment of the samples with an acetonitrile solution of UHP. The absence of a peak between 320–340 nm allowed to exclude formation of encapsulated diperoxo complexes [22]. Because UV–vis spectroscopy is unable to distinguish between different monoperoxo complexes, we attempted to elucidate the structure of monoperoxo complexes by Raman and XAFS spectroscopies.

Vibrational spectroscopy may be an attractive technique for the study of structures of peroxovanadium complexes. FT-IR studies of vanadium modified zeolites are restricted by the strong absorption of zeolites below 1100 cm^{-1}. On the other hand, the Raman spectrum of NaY is consisted of the only strong band at about 500 cm^{-1}, thus, facilitating detection of Raman scattering arose from encapsulated peroxovanadium species. In the $V–O_p$ vibrational region, the new bands at 549, 597 and 643 cm^{-1} appeared by treating $VO(pic)_2$–NaY (HL) with an acetonitrile solution of UHP (Fig. 3). $VO(pic)_2 \cdot H_2O$ and encapsulated vanadium bispicolinate showed similar peak position for V=O stretching (969 and 971 cm^{-1}, respectively), whereas $VO(pic)_2$–NaY (HL) treated with UHP showed shift and broadening of the band. The new band at 953 cm^{-1} may be attributed to O–O stretching. ν(O–O) bands for $H[VO(O_2)(pic)_2] \cdot H_2O$ and $VO(O_2)(pic) \cdot 2H_2O$ were observed at 939 and 934 cm^{-1}, respectively (Table 1). Thus, the Raman studies revealed transformation of the encapsulated vanadium bispicolinate complex to peroxovanadium species. However, comparison with the spectra for the reference peroxovanadium complexes did not allow to make conclusions about exact structure of the resultant vanadium species. Despite the similarity of positions of the new Raman bands to those for the monopicolinate structure $VO(O_2)(pic) \cdot H_2O$, their relative intensities are quite different with each other. In addition, the band at 678 cm^{-1} for $VO(O_2)(pic) \cdot H_2O$ was weak with the encapsulated species and its peak position could not be determined exactly as shown in Fig. 3c. It is established that in the V–O peroxo region,

Raman spectrum is highly sensitive towards changes in the coordination polyhedron of the complexes, and both the band positions and the intensities are characteristic features [27,28]. The distinct difference in the Raman spectra for the encapsulated peroxospecies and the reference compounds may be ascribed to difference in geometry of the complexes imposed by their location in zeolite supercages. The difference between two $V-O_p$ bands—643 cm^{-1} (ν_1) and 597 cm^{-1} (ν_2), for the encapsulated peroxovanadium complex, is 46 cm^{-1} which suggests a pentagonal bipyramidal coordination around vanadium in the peroxo complex [27,28].

It should be noted that the strong bands at about 980 and 880 cm^{-1} characteristics of hydrogen peroxide solution of vanadates (V=O and O–O stretchings in oxodiperoxo complexes) were clearly absent. The fact argues for retention of at least one picolinate ligand in the coordination sphere of the peroxovanadium complex, which stabilizes the monoperoxo structure. This is in agreement with the conclusion from UV–vis study. Although the structure of pentagonal bipyramidal vanadium monopicolinate monoperoxo complex was concluded, however, we cannot exclude bispicolinate peroxo species on the basis of the Raman study. The additional argument for monopicolinate monoperoxovanadium (V) complex was obtained from the in situ XANES study. The vanadium 4p level is easily perturbed by valence changes and also affected by ligand coordination [29]. Actually, position of the $1s \rightarrow 4p$ transition provides the information about the number of picolinic ligands in the vanadium monoperoxo complex. $H[VO(O_2)(pic)_2] \cdot H_2O$ (Fig. 4c) showed the $1s \rightarrow 4p$ transition peak at 5485.0 eV, whereas $VO(O_2)(pic) \cdot 2H_2O$ exhibited the peak at 5485.7 eV for (Fig. 4d). Comparison of these values with 5485.7 eV for the $VO(pic)_2$–NaY (HL) sample treated with UHP solution (Fig. 4b) allowed us to suppose the formation of monoperoxo complex with one picolinic ligand. Small difference in the edge shape between the sample and the reference complex in Fig. 4 may be explained by the presence of V(+4) picolinates in the sample. The EXAFS results did not give useful information on the structure, but did not contradict with the suggestion about formation of monoperoxo vanadium monopicolinate complex in the NaY zeolite [37].

4.3. Catalytic activity of encapsulated vanadium complexes

Catalytic chemistry of vanadium peroxo complexes containing pyridine-2-carboxylato ligands in solutions has been studied by Mimoun et al. [13] and Shul'pin and Süss-Fink [14] and Shul'pin et al. [15] in detail. They found that these compounds effectively catalyzed hydroxylation of aromatic and aliphatic hydrocarbons as well as oxidation of alcohols. Our spectroscopic studies proved the formation of monoperoxo picolinate species from NaY-encapsulated $VO(pic)_2$ complex upon UHP treatment which allowed us to expect catalytic activity of the $VO(pic)_2$–NaY sample similar to those of the peroxo picolinate complexes in solution. In fact, cyclohexane, 2-propanol and benzene were oxidized on $VO(pic)_2$–NaY (HL) catalyst to cyclohexyl hydroperoxide, acetone, and phenol, respectively. The encapsulated vanadium bispicolinate complex retained the solution-like behavior but the activity of the $VO(pic)_2$–NaY (HL) catalyst was $\sim$7–10 times lower than the activity of $H[VO(O_2)(pic)_2] \cdot H_2O$ under the similar reaction conditions. The results may be explained by either low diffusion rates of the reagents to active intrazeolitic center or formation of dimer species as reaction intermediates which is difficult in the case of encapsulated $VO(pic)_2$ complex.

4.4. Stability of encapsulated catalysts

It is well-established that peroxide ligand is strong enough to substitute ligands weakly bonded to vanadium [12,38]. This process can result in low stability of a vanadium catalyst

[39,40]. Noticeable leaching of vanadium to the solution was observed when 31% H_2O_2 was used as oxidant in spite of retention of at lest one picolinic ligand in the coordination sphere of vanadium atom. To minimize extraction of the encapsulated vanadium complexes into the solution, all reactions were carried out under anhydrous conditions and UHP was used as oxidant. However, we did not succeed in complete suppressing the leaching of vanadium. The contribution of homogeneous catalysis (30–50%) to the reactions was caused by leaching of 1–3% of the active vanadium complex into the solution. The best results were obtained with $VO(Qpic)_2$–NaY (LL) catalyst. A proposed mechanism for the complex leaching is pictured in Scheme 1. On the basis of the spectroscopic studies, we suggest the formation of monopicolinate complex that is fixed by spatial restrictions inside zeolite pore, but more weakly than in the case of $VO(pic)_2$ precursor. The preferable formation of monopicolinate complex can be explained by Coulombic interaction with zeolite lattice that is a driving force strong enough to cause dissociation of anionic bispicolinate monoperoxovanadium complex initially formed. The decrease in the activity was observed for spent catalyst though not much V loading decreased by XRF analysis, and might be ascribed to pore blockage by products that cannot be removed by washing with acetonitrile.

4.5. Shape selective effects

Usually, the zeolite catalysts show a number of shape selective effects due to mass transport discrimination phenomena (size selectivity) and due to restricted space in zeolite pores (regioselectivity and spatioselectivity) [3,41–43]. In fact, smaller molecules exhibited higher conversion rates as compared with bigger ones in the competitive oxidations. When the homogeneous catalyst $H[VO(O_2)(pic)_2] \cdot H_2O$ was displaced by the encapsulated catalyst $VO(pic)_2$–NaY (HL), the relative reactivities for the pairs of: cyclooctane: cyclodecane, toluene: 1,3-di-*t*-butylbenzene, and *n*-octane: 2,5-dimethylhexane increased by 14, 15 and 6%, respectively. It should be noted that the best reported 'ship-in-a-bottle' catalysts showed only 20–40% increase in the relative rate of cyclohexane oxidation in the cyclohexane: cyclododecane competitive oxidation [3,43]. Thus, the absence of remarked effects can be explained by both multicomponent diffusion [44] and leaching of catalytically active component.

The other shape selective effect in the catalytic system involved changes in regioselectivity in hydrocarbon oxidations. Alicyclic alkanes behaved as a rod poked through the zeolite channel so that the end of rod will be the first to reach catalytic center. In the case of vanadium picolinate catalysts, use of the encapsulated

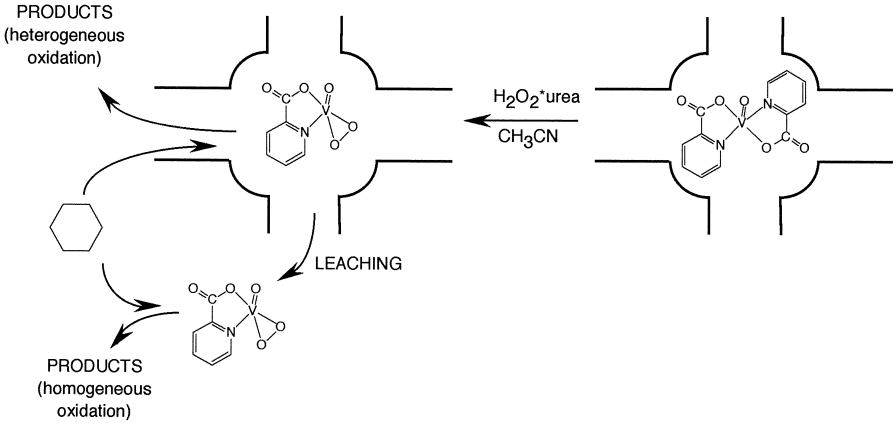

Scheme 1. Schematic representation of heterogeneous and homogeneous reaction pathways in cyclohexane oxidation on the encapsulated $VO(pic)_2$-NaY catalyst.

$VO(pic)_2$–NaY (HL) did not cause significant change of regioselectivity in *n*-alkane oxidations (*n*-hexane and *n*-octane) in comparison with homogeneous $H[VO(O_2)(pic)_2] \cdot H_2O$ catalyst. For example, for *n*-octane a little increase of the amounts of C_1-position oxidation products was observed. The selectivity of oxidation of terminal CH_3- group is close to that observed for large pore (~0.7 nm) vanadium silicate V-NCL-1, but significantly lower than for medium pore (~0.54–0.56 nm) VS-1 and VS-2 (Table 2) [30–32,45]. More noticeable effects were found for reaction of 2,5-dimethylhexane hydroxylation on the encapsulated vanadium picolinate catalysts. The encapsulated $VO(pic)_2$–NaY (LL) catalyst showed two times larger selectivity (position 1/position 3) as compared with a homogeneous counterpart.

One of characteristic features in the oxidations by the encapsulated $VO(PL)_2$–NaY catalyst was the preferable formation of alkyl hydroperoxides, whereas homogeneous oxidation produced significant amounts of carbonyl products. In other words, the encapsulated catalyst allowed to predict the transformation of primarily formed hydroperoxides to carbonyl compounds. This is in agreement with inactivity of $VO(pic)_2$–NaY (HL) when *t*-BuOOH was used as oxidant. The selective formation of alkyl hydroperoxides is probably imposed by location of vanadium in supercage that restricts the interaction of alkyl hydroperoxides with intrazeolitic vanadium sites. Such behavior of the novel $VO(PL)_2$–NaY catalysts is opposite to that of transition metal silicates which shows great activity in secondary oxidation reactions (Table 2) [30–33,45].

4.6. Mechanism of aliphatic hydrocarbon oxidations on encapsulated $VO(pic)_2$–NaY catalysts

Spectroscopic studies proved the formation of monoperoxovanadium species that could be actual oxidants regenerating with H_2O_2 in a catalytic manner. Product distribution in isomeric octane oxidations, namely, formation of relatively large amounts of the CH_3- oxidation product allows us to suppose that a key role in the transformation of alkane into hydroperoxide is played by O-centered radicals, i.e., hydroxyl radical or vanadium-containing radical species [14,46]. On the other hand, variation in regioselectivity as well as failure of catalytic oxidation with *t*-BuOOH allow to reject a dominating role of $HO\cdot$ radical species in the process. The radical mechanism is also supported by the results of toluene oxidation where a significant amount of *m*-cresol is formed. Most probable mechanism of generation of the O-centered radicals from monoperoxovanadium species involves intramolecular electron transfer to give V^{IV}–$OO\cdot$ [13,14]. This radical is capable to abstract a hydrogen atom of RH to form $R\cdot$ that can react with molecular oxygen or abstract OOH from a vanadium hydroperoxide VOOH. The final step should involve regeneration of vanadium peroxo complexes with H_2O_2.

5. Conclusions

Treatment of the $VO(pic)_2$–NaY (HL) zeolite with an acetonitrile solution of urea hydrogen peroxide adduct allowed to generate monoperoxovanadium species which was found to be active intermediate for various catalytic oxidation reactions. The novel ‘ship-in-a-bottle’ catalyst retained solution-like activity for aliphatic and aromatic hydrocarbon oxidations as well as for alcohol oxidations. Alkane oxidations on the encapsulated vanadium bispicolinate catalysts proceeded via formation of a monoperoxo vanadium complex by radical mechanism. The $VO(pic)_2$–NaY (HL) catalyst showed preferable oxidation of smaller substrates in competitive oxidations. The selectivity of oxidation of terminal CH_3- group in isomeric octanes was larger for the encapsulated catalyst than for the homogeneous catalyst. Another feature of the encapsulated catalysts was preferable (sometimes exclusive) formation of alkyl hydroperoxides in alkane oxidations. The features

may be explained in terms of intrazeolitic location of the active complexes. Low stability of the catalysts against leaching is caused by the formation of monoperoxo complex containing only one picolinic ligand.

Acknowledgements

The authors thank Prof. H. Shindo, Chuo University, for helping us in measuring Raman spectra. This work has been supported by CREST (Core Research for Evolutional Science and Technology) of JST (Japan Science and Technology).

References

[1] R.A. Sheldon, J.D. Chen, J. Dakka, E. Neeleman, Stud. Surf. Sci. Catal. 82 (1994) 515.
[2] P.B. Venuto, Microporous Mater. 2 (1994) 297.
[3] D.R.C. Huybrechts, R.F. Parton, P.A. Jacobs, in: T. Inui, S. Namba, T. Tastumi (Eds.), Chemistry of Microporous Crystals, Stud. Surf. Sci. Catal. 60, Elsevier, Amsterdam, 1991, p. 225.
[4] G. Bellussi, M.S. Rigutto, Stud. Surf. Sci. Catal. 85 (1994) 177.
[5] K.J. Balkus Jr., A.G. Gabrielov, J. Inclusion Phenom. Mol. Recognit. Chem. 21 (1995) 159.
[6] D.E. De Vos, F. Thibault-Starzyk, P.P. Knops-Gerrits, R.F. Parton, P.A. Jacobs, Macromol. Symp. 80 (1994) 157.
[7] D.E. De Vos, P.P. Knops-Gerrits, R.F. Parton, B.M. Weckhuysen, P.A. Jacobs, R.A. Schoonheydt, J. Inclusion Phenom. Mol. Recognit. Chem. 21 (1995) 185.
[8] B. Romanovsky, Macromol. Symp. 80 (1994) 185.
[9] P.P. Knops-Gerrits, D.E. De Vos, P.A. Jacobs, J. Mol. Catal. A: Chem. 117 (1997) 57.
[10] K.J. Balkus Jr., A.K. Khanmamedova, K.M. Dixon, F. Bedioui, Appl. Catal. A: Gen. 143 (1996) 159.
[11] A. Butler, M.J. Clauge, G.E. Meister, Chem. Rev. 94 (1994) 625.
[12] V. Conte, F. Di Furia, G. Licini, Appl. Catal. A: Gen. 157 (1997) 335.
[13] H. Mimoun, L. Saussine, E. Daire, M. Postel, J. Fischer, R. Weiss, J. Am. Chem. Soc. 105 (1983) 3101.
[14] G.B. Shul'pin, G. Süss-Fink, J. Chem. Soc. Perkin Trans. 2 (1995) 1459.
[15] G.B. Shul'pin, D. Attanasio, L. Suber, J. Catal. 142 (1993) 147.
[16] A. Kozlov, K. Asakura, Y. Iwasawa, Chem. Lett. (1997) 313.
[17] A. Kozlov, K. Asakura, Y. Iwasawa, J. Chem. Soc. Faraday Trans. 94 (1998) 809.
[18] K. Maruszewski, D.P. Strommen, K. Handrich, R. Kincaid, Inorg. Chem. 30 (1991) 4579.
[19] R.L. Dutta, S. Ghosh, J. Indian Chem. Soc. 44 (1967) 271.
[20] K. Asakura, in: Y. Iwasawa (Ed.), X-ray Absorption Fine Structure for Catalysts and Surface, World Scientific, Singapore, 1996, p. 33.
[21] A. Samuni, G. Czapski, Isr. J. Chem. 8 (1970) 563.
[22] M. Sivák, H. Gécilová, Acta F.R.N. Univ. Comen.-Chimia 35 (1987) 81.
[23] C. Brémand, D. Bougeard, Adv. Mater. 7 (1995) 10.
[24] P.P. Knops-Gerrits, D.E. De Vos, E.J.P. Feijen, P.A. Jacobs, Microporous Mater. 8 (1997) 3.
[25] P. Schwendt, M. Sivák, A.E. Laphin, Yu.I. Smolin, Yu.F. Shepelev, D. Gyepesová, Transition Metal Chem. 19 (1994) 34.
[26] N.J. Campbell, A.C. Dengel, W.P. Griffith, Polyhedron 8 (1989) 1379.
[27] P. Schwendt, M. Pisárcik, Chem. Pap. 42 (1988) 305.
[28] P. Schwendt, K. Volka, M. Suchánek, Spectrochim. Acta 44A (1988) 839.
[29] J. Wong, F.W. Lytle, R.P. Messmer, D.H. Maylotte, Phys. Rev. B 30 (1984) 5596.
[30] A.P. Singh, T. Selvam, J. Mol. Catal. A: Chem. 113 (1996) 489.
[31] P.R.H.P. Rao, A.V. Ramaswamy, P. Ratnasamy, J. Catal. 141 (1993) 604.
[32] K.R. Reddy, A.V. Ramaswamy, P. Ratnasamy, J. Catal. 143 (1993) 275.
[33] M.G. Clerici, Appl. Catal. 68 (1991) 249.
[34] R.A. Sheldon, J.K. Kochi, Adv. Catal. 25 (1976) 274.
[35] T.R. Boehlow, Ch.D. Spilling, Tetrahedron Lett. 37 (1996) 2717.
[36] W. Adam, R. Kumar, T.I. Reddy, M. Renz, Angew. Chem. Int. Ed. Engl. 35 (1996) 880.
[37] A.I. Kozlov, Doctoral Thesis, The University of Tokyo, September 1997.
[38] E.P. Talsi, New J. Chem. 21 (1997) 709.
[39] J.S. Reddy, P. Liu, A. Sayari, Appl. Catal. A: Gen. 148 (1996) 7.
[40] I.W.C.E. Arends, M. Pellizon, R.A. Sheldon, Stud. Surf. Sci. Catal. 110 (1997) 1031.
[41] N.Y. Chen, W.E. Garwood, Dwyer, F.G., Shape Selective Catalysis in Industrial Applications, Marcel Dekker, New York, 1989.
[42] D.R. Corbin, N. Herron, J. Mol. Catal. 86 (1994) 343.
[43] N. Herron, J. Coord. Chem. 19 (1988) 25.
[44] S.S. Nivarthi, H.T. Davis, A.V. McCormick, Chem. Eng. Sci. 50 (1995) 3217.
[45] P.R.H.P. Rao, K.R. Reddy, A.V. Ramaswamy, P. Ratnasamy, Stud. Surf. Sci. Catal. 78 (1993) 385.
[46] G.V. Nizova, G.B. Shul'pin, Russ. Chem. Bull. 43 (1994) 1146.